ELSEVIER

Journal of Neuroscience Methods 78 (1997) 105–113

JOURNAL OF NEUROSCIENCE METHODS

A simple hardware model for the direct observation of voltage-clamp performance under realistic conditions

A. Draguhn [a,*], M. Pfeiffer [a], U. Heinemann [a], R. Polder [b]

[a] *Institut für Physiologie der Charité, Tucholskystr. 2, D-10117 Berlin, Germany*
[b] *NPI Electronic GmbH, Haeldenstr. 62, D-71732 Tamm, Germany*

Received 2 April 1997; received in revised form 30 July 1997; accepted 13 August 1997

Abstract

A new hardware cell model for electrophysiological recording has been constructed which allows for the assessment of voltage clamp accuracy in different recording situations. Each compartment consists of a capacitor in parallel with a variable resistor and can be connected to other compartments by a variable axial resistance. The simulated membrane resistance can be changed extrinsically by a command voltage input which is optically coupled to the cell without any direct galvanic contact. Each compartment possesses a buffer amplifier which reads out the potential at the simulated membrane element, (e.g. 'somatic' or 'dendritic' potential). The model allows for the direct observation of typical situations and problems arising in electrophysiological experiments. We used the model to monitor deviations between the 'intracellular' and the command voltage, e.g. due to series resistance errors. We also used the model to simulate synaptic currents which were generated by triangular membrane conductance changes. The results demonstrate the strong influence of synaptic location and series resistance on voltage clamp fidelity. The cell model is a new and easy-to-handle tool for the observation of voltage control under realistic experimental conditions. © 1997 Elsevier Science B.V.

Keywords: Cell model; Voltage clamp; Patch clamp; Synaptic current; Simulation

1. Introduction

Voltage clamp (VC) methods are widely used for the analysis of the electrical behaviour of cells, mainly because they provide information about the membrane conductance under defined electrostatic and—in patch-clamp experiments—ionic conditions. At constant membrane potential, the conductance is directly proportional to the observed current and therefore the data can be easily interpreted in terms of ion channels or electrogenic pumps.

VC experiments on small cells are usually performed with a single electrode which is used for both potential measurement and for the injection of current. Two different amplifier designs are currently used for this type of experiments. 'Switched' single electrode voltage clamp amplifiers change at high frequency between potential measurement and current injection (Brennecke and Lindemann, 1974; Wilson and Goldner, 1975). The intracellular potential is measured during the current-free interval when the voltage transient occurring at the electrode tip during current injection has completely relaxed. Such discontinuous VC-amplifiers (dSEVC) have been used in numerous experiments for the analysis of transmitter- or voltage-gated conductance changes, both with sharp intracellular microelectrodes and with suction pipettes in the whole-cell configuration of the patch-clamp technique (for comparison, see Staley et al., 1992). An alternative amplifier design allows for VC-recording at extremely low noise levels. This type (cPCA for continuous-feedback patch-clamp amplifier) presets the potential at the electrode to the command potential (V_{cmd}) and continuously injects

* Corresponding author. Tel.: +49 30 28026613/6640; fax: +49 30 28026669; e-mail: draguhn@rz.charite.hu-berlin.de

PII S0165-0270(97)00138-6

current into the pipette to correct for voltage deviations (Hamill et al., 1981; Marty and Neher, 1995; Sigworth, 1995).

An ideal experimental situation for whole cell recordings requires a simple (e.g. spherical) and small cell with high membrane resistance (R_m) and a low resistance between the electrode interior and the cell (series resistance, R_{series}). Real experiments rarely meet these conditions. In cPCA recordings, the voltage divider formed by R_m and R_{series} can cause severe deviations of the intracellular potential from V_{cmd} if not $R_{series} \ll R_m$. Moreover, R_{series} and C_m form a low-pass filter which can significantly distort the time-course of VC signals (Ogden and Stanfield, 1994). The use of dSEVCs can largely eliminate these errors, but this advantage is usually paid for with enhanced noise. Such recordings can also suffer from low bandwidth if the pipette configuration or the design of the capacitance compensation circuit are unfavourable.

Many voltage clamp experimenters work with complex cells which cannot be modelled by a single compartment. In addition to the problems mentioned above, the presence of more remote compartments like dendrites or axons causes an inhomogeneous voltage control in the cell (Armstrong and Gilly, 1992; Müller and Lux, 1993). Areas located close to the soma will follow the command voltage with higher speed and fidelity than remote compartments. Conductance changes occurring in peripheral parts will be distorted both in amplitude and time. This problem, known as the 'space clamp' problem, is of particular importance for the recording of synaptic currents and has been addressed in detail by various authors, both experimentally (Silver et al., 1992; Bekkers and Stevens, 1996; Williams and Johnston, 1991) and in theoretical models (Major, 1993; Spruston et al., 1993).

Recently, Sala and Sala (1994) directly compared both different VC amplifier designs (dSEVC and cPCA) in a computer simulation. Whereas such theoretical models can help to understand the parameters influencing voltage clamp recordings in great detail, they do not allow to control directly the VC performance of the machinery and electrode configuration used in real experiments. Recordings from living cells, on the other hand, give usually no direct information about the size and location of potential deviations from the desired V_{cmd}. We have, therefore, constructed a new hardware cell model with the following properties: The model consists of RC-compartments which can be coupled by variable resistors to simulate multi-compartment cells. The simulated membrane resistance R_m can be changed by an externally controlled infrared LED-device. This galvanically isolated device allows for complex and rapid changes of R_m (e.g. simulating synaptic conductance changes) without any extension of the actual circuit simulating the cell's membrane resistance and capacitance. The potential inside each compartment (e.g. 'somatic' or 'dendritic') is directly measured and read out via a high-impedance operational amplifier. A similar model has already been used in combination with a real recording chamber and microelectrodes to demonstrate the voltage- and current clamp performance of a dSEVC in unusually deep preparations (Richter et al., 1996).

Here we describe three typical applications of the model: we compare the sensitivity of two different types of amplifiers to series resistance, demonstrate the loss of voltage control in a complex (two compartment) cell and directly measure the stability of the intracellular potential in voltage clamp recordings of 'synaptic' conductance changes.

2. Materials and methods

2.1. Construction of the test cell

The cell model consists of individual RC-elements which can be interconnected by variable resistors to simulate multi-compartment cells. Each RC-element has a given capacitance C_m in parallel with a variable resistor, R_m, which is controlled by an infrared LED device (H11F1, General Electric Company, Auburn, NY, USA; Sahm III and Smith, 1984). Thus, R_m can be changed by an external command voltage without any galvanic extension of the membrane-simulating circuit. In order to achieve largely linear changes of R_m with the command voltage $V(R)$, the LED is controlled by a feedback loop (Fig. 1A) which is individually adjusted for each model cell. In addition, the 'intracellular'

Fig. 1. Scheme of the variable resistor and the test cell recording setup. (A) Each compartment contains a variable resistor (R_m) which is controlled by an infrared light-emitting diode coupled to a symmetrical bilateral silicon photo detector. The detector is electrically isolated from the input and performs like an ideally isolated field effect transistor. The low level output characteristic of FET devices has a region of linear resistance which can be controlled by an external signal. Here, the resistance can be varied by the current applied to the LED. The nonlinear relationship between LED current and output resistance is linearised in the electronic feedback loop. The output range is from a few kΩ to hundreds of MΩ with input voltages of a few V. The resistance can be controlled by changing $V(R)$ at the potentiometer or the BNC-input. A high-impedance buffer amplifier reads out the voltage at the variable resistor mimicking R_m. (B) Scheme of a two-compartment version of the test cell. Both compartments are coupled via a variable axial resistor and the voltage can be recorded from both compartments at the buffer amplifier. The series resistance is mimicked by another variable resistor. (C) Recording setup. The individual components are connected in series with the amplifier and the resistance in each compartment is controlled by an external DC-voltage source. V_{soma} and $V_{dendrite}$ are the intracellular potentials read out by the buffer amplifiers which can be compared to the voltage V read out by the amplifier.

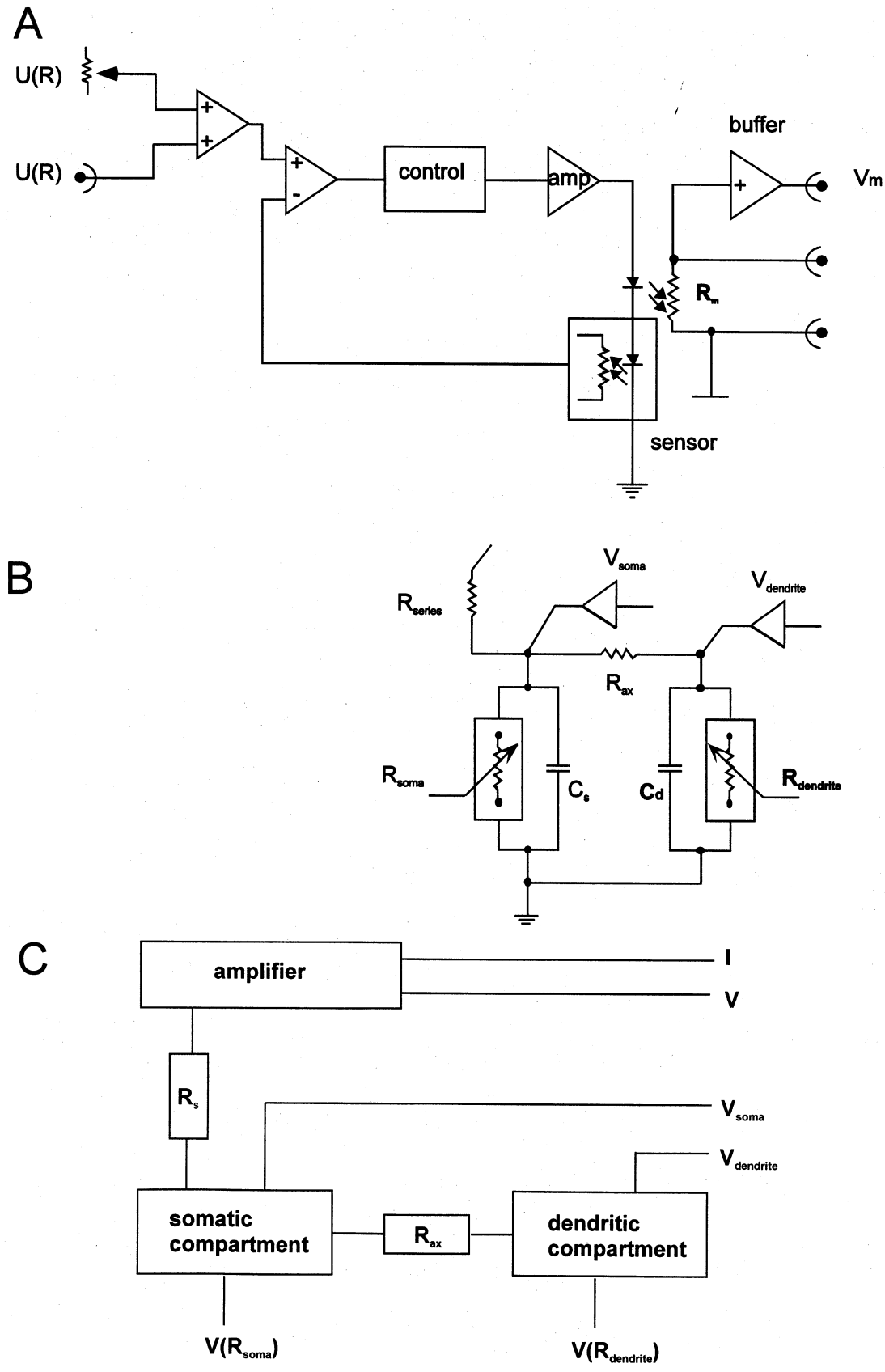
A
U(R)
U(R)
control
amp
buffer
Vm
Rm
sensor
B
Rseries
Vsoma
Vdendrite
Rax
Rsoma
Cs
Cd
Rdendrite
C
amplifier
I
V
Rs
Vsoma
Vdendrite
somatic compartment
Rax
dendritic compartment
V(Rsoma)
V(Rdendrite)

Fig. 1.

potential is monitored by a high-impedance buffer-amplifier. Thus, deviations between the command potential and the actual potential within each compartment can be continuously monitored. The pipette resistance and axial resistances between the simulated compartments have been simulated by conventional potentiometers in separate metal cases. The complete original circuit diagram of the cell model can be obtained from the corresponding author on request.

Single- or multi-compartment cell models can be constructed with the elements. We will use the nomenclature given in Fig. 1B: R_m and C_m are the modelled membrane resistance and capacitance, respectively, which are indexed with the appropriate compartment where necessary (R_{soma}, $C_{dendrite}$ etc.). R_{series} is the series or access resistance between the amplifier input and the cell interior, R_{ax} is the axial resistance between the first and the second compartment, $V(R)$ is the command voltage determining the actual value of the optically isolated resistor, V_{cmd} the VC command potential and R_{input} is the apparent input resistance of the cell model. R_{input} is calculated as 10 mV divided by the DC current injected during a 10 mV command voltage step.

2.2. Electrophysiological measurements

The test cell was connected to the VC-amplifier by a variable resistor (1..20 MΩ) mimicking R_{series} (Fig. 1C). Two types of amplifier were used: an EPC-7 (HEKA electronic, Lambrecht, Germany) with a continuous feedback circuit and a dSEVC (SEC-5, NPI Electronic, Tamm, Germany). Series resistance compensation was employed in the cPCA recordings as indicated in results. When all elements were shielded by grounded metal boxes, the stray capacitance was 6.1 ± 2.0 pF and could be routinely compensated as in usual recordings. The VC performance of the dSEVC was optimized by adjusting gain and switching frequency. As in recordings from biological preparations, the electrode artefact settled within less than 3 μs so that switching frequencies of 35 to 45 kHz could be routinely used (compare Richter et al., 1996, Fig. 1). Data were recorded on an IBM-compatible computer with the TIDA program and ITC-16 interface (HEKA, Germany). We monitored the current, the voltage at the amplifier's potential output and the potential(s) read out by the buffer amplifier(s) in each of the artificial cell compartments. Usually, the holding potential was set to -20 mV throughout the experiments. VC control and intrinsic properties of the model cell were assessed by positive going 10 mV command voltage pulses. In these experiments, current was filtered by a four-pole Bessel low-pass filter at 8 kHz and the sample frequency was 20 kHz. Input resistance R_{input} was calculated from the steady-state current required to perform the 10 mV voltage step and was varied by external voltage commands to the variable optically coupled resistor R_m. For simulations of 'synaptic' currents we applied triangular command voltages ($V(R)$) to the optically isolated resistor R_m (see Fig. 6). The amplitude was adjusted to yield a 10 nS peak conductance change (200 pA current amplitude at -20 mV V_{cmd}). 'Synaptic' currents were filtered at 3 kHz and sampled at 8 kHz. For analysis and graphics, 20 traces of each experiment were superimposed and averaged.

3. Results

We employed the active cell model in different configurations to simulate typical experimental situations during whole-cell patch clamp recording. The individual elements of the test cell were included into the recording setup as schematically shown in Fig. 1C. In addition to the current and potential output of the amplifier, the true 'intracellular' potential in each compartment was continuously monitored and recorded from the buffer amplifier output (Fig. 1).

In a first series of measurements we used a compact single-compartment cell with $C_m = 33$ pF. The current and voltage responses to rectangular 10 mV command voltage pulses were measured at various values of R_m. Fig. 2 shows current and intracellular voltage traces recorded with a cPCA (EPC-7) at 10 MΩ series resistance. Partial compensation of R_{series} greatly improves the DC-voltage control in the cell interior as well as the speed of response. We recorded voltage step responses from the compact cell at three different series resistances (2, 5 and 10 MΩ, respectively) and with both a cPCA and a dSEVC (Fig. 3). Whereas a relatively tight cell (R_{input} 200–500 MΩ) follows the command pulse with high fidelity under voltage-clamp by a cPCA, severe deviations from $V_{command}$ occur at lower input resistance values. The error is strongly dependent on the series resistance and can be reduced by the activation of series resistance compensation or by employing a dSEVC (Fig. 3).

Many cells used in electrophysiological experiments (e.g. neurons) have a complex geometry which can not be mimicked by a single compartment composed of R_m in parallel with C_m. As a first approximation to more realistic cells we therefore added a second compartment to the model which is a simple hardware realization of the two-patch model developed by Armstrong and Gilly (1992). The proximal ('somatic') compartment had a capacitance of $C_{soma} = 33$ pF and the remote ('dendritic') compartment had a capacitance $C_{dendrite}$ of 180 pF. The membrane resistances in both compartments could be altered independently between 500 and 10 MΩ by external commands. Both compartments were separated by an inner axial resistance R_{ax} which could be varied manually between 2 and 20 MΩ (com-

pare Marty and Neher, 1995; Mainen and Sejnowski, 1996). Fig. 4 shows the step response of the two-compartment cell model recorded with a dSEVC at three different dendritic resistances. Series resistance was 5 MΩ and R_{ax} was 10 MΩ. Whereas the somatic voltage follows the command pulse relatively fast and complete, the dendritic potential increase does not reach the full command voltage amplitude when the remote compartment becomes leaky.

Fig. 5 summarizes the data obtained with command voltage jumps in recordings from the two-compartment cell model. Decreases in dendritic conductance cause a severe loss of voltage control in the dendritic compartment whereas the somatic voltage follows $U_{command}$ at all input resistances tested (Fig. 5A). In contrast, a somatic shunt (low R_{soma}) leaves the voltage control relatively unaffected in recordings with the dSEVC (Fig. 5B). In order to look at the dependence of voltage

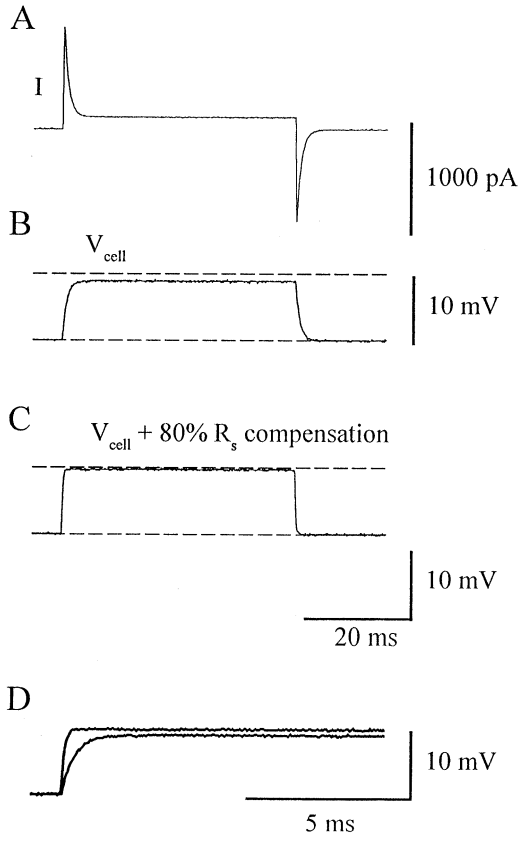

Fig. 2. Step response of test cell in a voltage clamp experiment with a continuous feedback patch-clamp amplifier (EPC-7). Single-compartment cell model with $C_m = 33$ pF, $R_{input} = 100$ MΩ and $R_{series} = 10$ MΩ. The command voltage was changed stepwise from −20 mV to −10 mV for 20 ms. (A) Current response. The peak response amplitude is approximately 1 nA corresponding to 10 MΩ series resistance. (B) Somatic voltage as read out by the buffer amplifier. Dashed line represents 10 mV. Note the marked delay before reaching a plateau and the remaining DC-error. (C) Somatic voltage response after activation of series resistance compensation results in a faster response with virtually no DC-error. (D) Superposition of the somatic voltage with and without R_{series}-compensation.

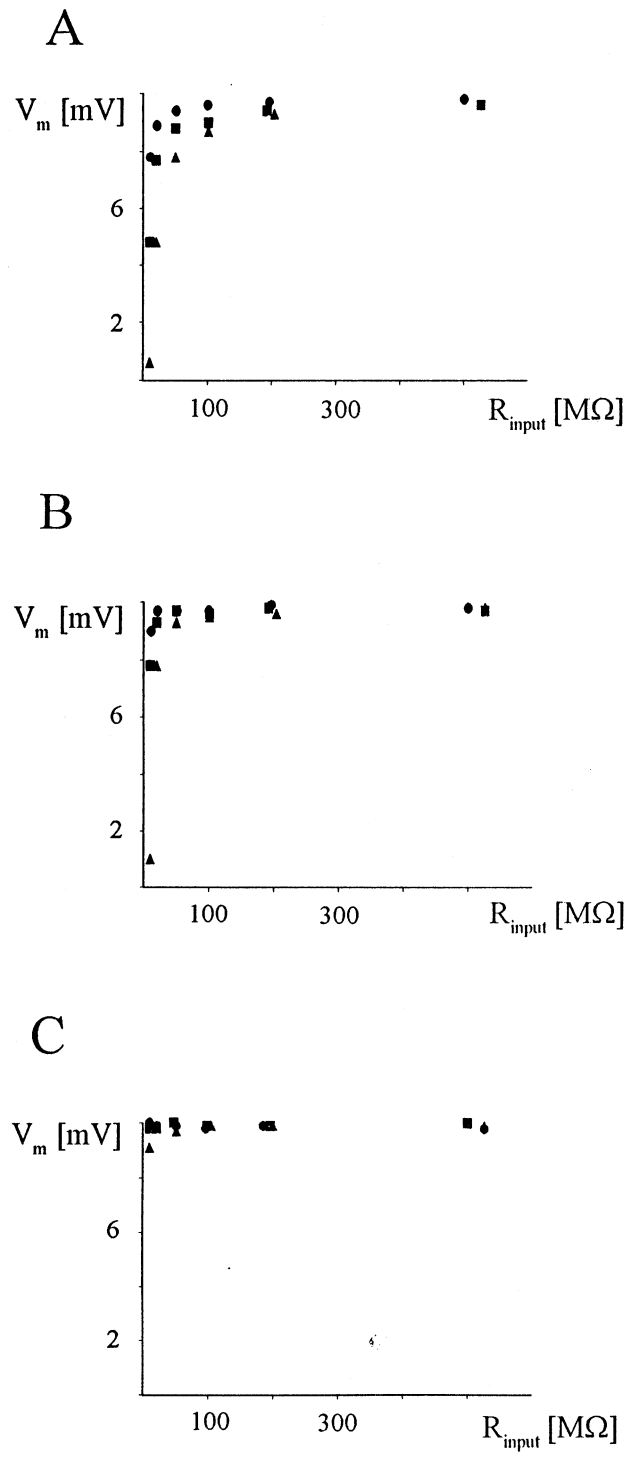

Fig. 3. Intracellular plateau voltage at different input resistances. (A) Voltage response to 10 mV command voltage step in a compact cell recorded with a continuous feedback amplifier without R_{series}-compensation. $R_{series} = 2$ MΩ (●), 5 MΩ (■) and 10 MΩ (▲). Note the marked decrease in voltage control at low input resistance. (B) The fidelity of response increases markedly after activating 80% series resistance compensation. (C) Performance of a 'switched' dSEVC is almost independent from both R_{series} and R_{input}.

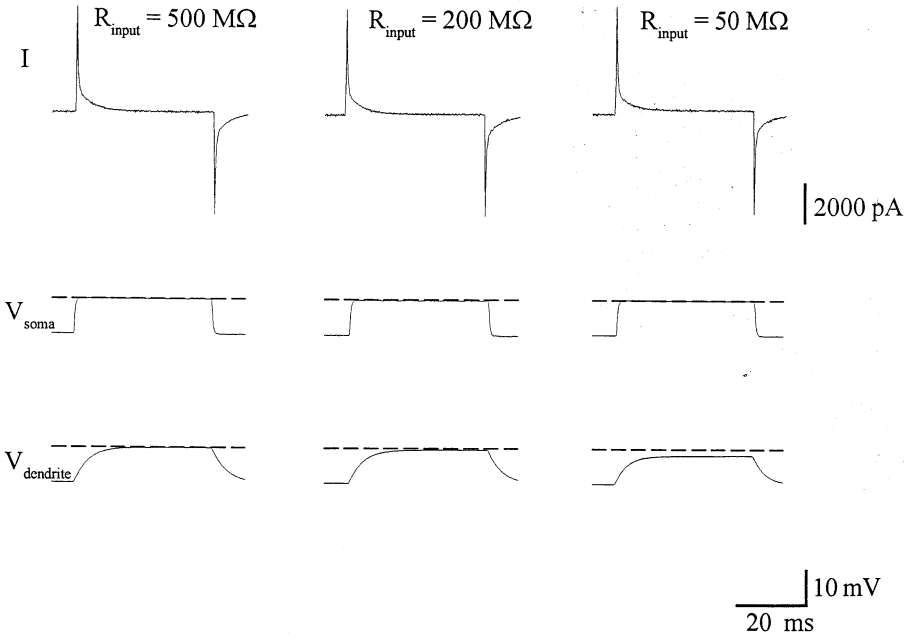

Fig. 4. Response of a two-compartment cell model to 10 mV command voltage steps. Recordings with a dSEVC at various total input resistances. Somatic compartment was constantly 500 MΩ and 33 pF, the dendritic resistance value was varied and dendritic capacitance $C_{dendrite}$ was 180 pF. Upper traces show the current response. Note the marked biexponential time course due to the different speed of charging in both compartments. Middle trace shows the voltage as read out by the buffer amplifier in the proximal ('somatic') compartment. VC-performance is almost independent from R_{input}. Bottom traces: Voltage control in a remote dendritic compartment is slow and shows some DC-deviation at low input resistances.

control from cell architecture, we then changed the inner resistance R_{ax} which separates the somatic and dendritic compartment (Fig. 5C). The data show that the dendritic voltage control decreases almost linearly when R_{ax} is increased. When somatic and dendritic compartment are separated by 20 MΩ, the 10 mV command voltage step results in only 6.8 mV dendritic voltage change. The time constant for completing the voltage change in the soma was between 0.16 and 0.22 ms at all values of R_{ax} In contrast, dendritic charging was very sensitive to changes of the inner resistance ranging from $\tau = 0.47$ ms ($R_{ax} = 2$ MΩ) to $\tau = 2.93$ ms ($R_{ax} = 20$ MΩ).

Many voltage clamp experiments are not designed to impose command voltage steps on the cell but often try to register membrane conductance changes at a stable membrane potential, e.g. due to the opening of transmitter-gated ion channels. These recordings can be severely compromised by series resistance or due to a complex cell geometry. We, therefore, altered the simulated dendritic membrane resistance at a constant holding potential (-20 mV) to mimic a synaptic conductance change of 10 nS. Fig. 6 shows recordings with a cPCA (EPC-7) at varying series resistances. The distortion of the current kinetics and reduction of amplitude are obvious when R_{series} is increased from 2 to 20 MΩ. The cell model allows for the direct inspection of the somatic and dendritic voltage escape which can reach significant values. At $R_{series} = 20$ MΩ the dendritic voltage deviates by 3.6 mV from V_{cmd}, whereas in current clamp the 'postsynaptic' potential reaches 8.2 mV. Thus, the voltage clamp reduces the synaptic potential fluctuations by only 56% under these conditions. The somatic voltage escape is still 2.5 mV (compared to 8.1 mV in CC) under these conditions. However, the direct comparison of the intracellular potential in CC vs. VC recording at 20 MΩ series resistance shows that even under unfavourable VC conditions the potential deviation is drastically shortened in VC recordings (Fig. 6D). The VC data (clamp current amplitude, somatic and dendritic voltage escape at varying R_{series}) are summarized in Fig. 7A. The effect of series resistance on the somatic voltage escape can be largely overcome by use of a dSEVC. However, there is still significant voltage escape in remote compartments leading to underestimation of the synaptic conductance change (Fig. 7B).

4. Discussion

Hard-wired cell models are routinely used in electrophysiology for calibration procedures, tests of equipment or in order to demonstrate basic intrinsic properties of cell membranes. However, these simple RC-circuits are usually not very versatile and do not allow to check the quality of the voltage clamp in a realistic recording situation.

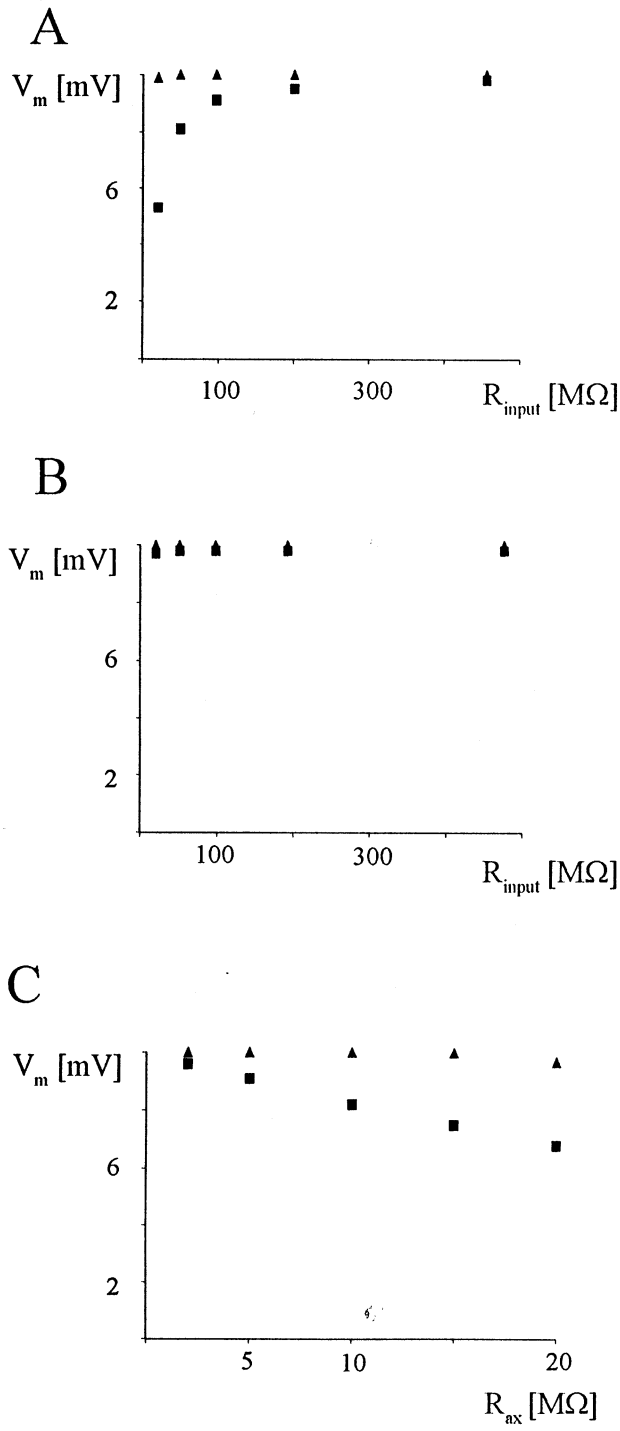

Fig. 5. Somatic (▲) and dendritic (■) voltage following a 10 mV command voltage pulse. Recordings with dSEVC at $R_{series} = 5$ MΩ. A: Input resistance was varied by variation of $R_{dendrite}$ with constant R_{soma} (500 MΩ). Axial resistance 10 MΩ. Note loss of dendritic (DC) voltage control with decreasing resistance. B: Variation of somatic resistance, $R_{dendrite} = 500$ MΩ = const. Axial resistance 10 MΩ. Somatic leak does not deteriorate voltage control in a cell clamped with a dSEVC. C: Change of voltage control following variation of the axial resistance between 'soma' and 'dendrite'. Increasing R_{ax} results in decreasing DC voltage control in the remote compartment.

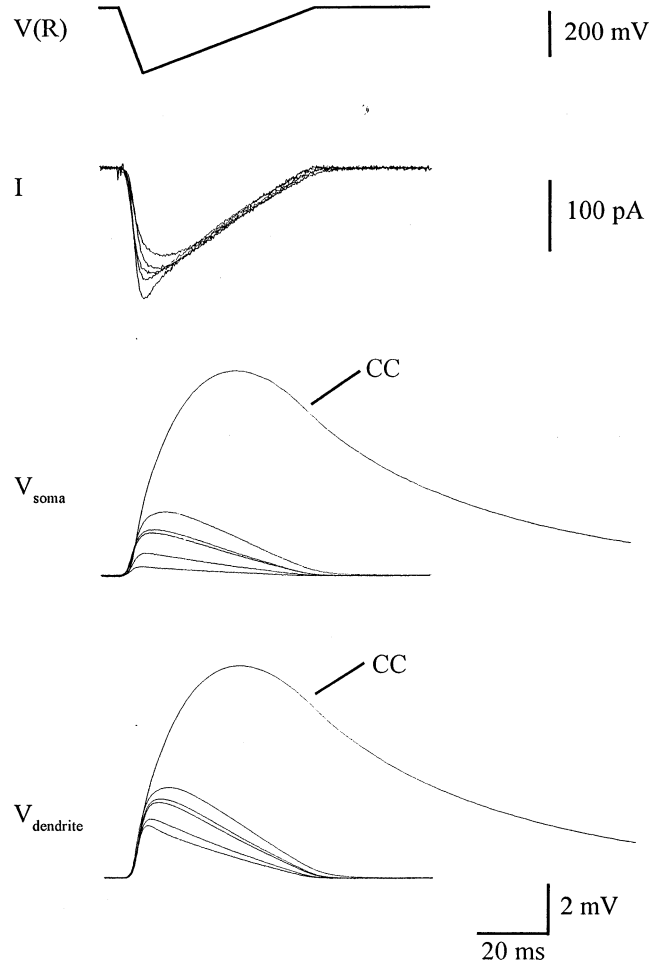

Fig. 6. Current, somatic and dendritic voltage escape following a triangular decrease of R_{input} in the remote ('dendritic') compartment. Recordings were performed with a continuous feedback patch-clamp amplifier at varying series resistances of 2, 5, 10, 15 and 20 MΩ, respectively. $R_{soma} = R_{dendrite} = 500$ MΩ. Maximal dendritic conductance change corresponding to 10 nS. Upper trace shows the extrinsic command voltage applied to alter the membrane resistance. Increasing the series resistance results in decreased current amplitude and velocity (I) and in increased somatic and dendritic volatege escape. Note for comparison the voltage deviations recorded under CC conditions for the same conductance change.

The cell model presented in this paper has two new and unique features. Firstly, the voltage within each compartment can be read out from a built-in buffer amplifier and secondly, R_m can be altered extrinsically by application of a command voltage. The buffer amplifier has a high input impedance and therefore does not change the current flow through the model. The variable resistor R_m is galvanically separated from the control circuit and can be changed by photon-coupled FET devices. This allows for the simulation of complex patterns of conductance changes (like synaptic inputs) while the galvanic separation of control circuit and R_m ensures that the connection of the cell with an external voltage source has no influence on the current flow and potentials within the RC-compartment.

We used the model cell in a series of different experiments demonstrating fundamental properties and problems of VC recordings. Responses to square command voltage jumps are frequently used to measure the passive properties of the cell membrane. In recordings with a cPCA the current response will allow for the calculation of the cell's input resistance R_{input} ($R_m + R_{series}$) and for an estimate of the series resistance R_{series}, which can be calculated from the peak amplitude of the current transient or from the current decay time constant (Armstrong and Gilly, 1992) as long as $R_{series} \ll R_m$. The time course of the charging current also gives information about the speed with which the cell will adopt a new membrane potential after a command voltage step. However, the intracellular potential cannot be directly measured in cPCA recordings and might be considerably delayed towards V_{cmd} or might not reach the full amplitude defined by V_{cmd}. The test cell model allows for the direct observation of the 'intracellular' voltage and, thus, can demonstrate the influence of R_{series}, membrane conductance and cellular geometry on VC quality. We demonstrated the increasing DC-errors caused by R_{series} at increased membrane conductance, e.g. in 'leaky' cells or after activation of large currents, such as voltage-dependent sodium or potassium currents (Armstrong and Gilly, 1992). The cell model can also be used to document the frequency-dependent error caused by the series resistance. R_{series} and C_m form a low-pass filter with the corner frequency $f_c = (2^{**} R_{series} C_m)^{-1}$ (for $R_{series} \ll R_m$) which can drastically reduce the bandwidth of the recordings (Ogden and Stanfield, 1994).

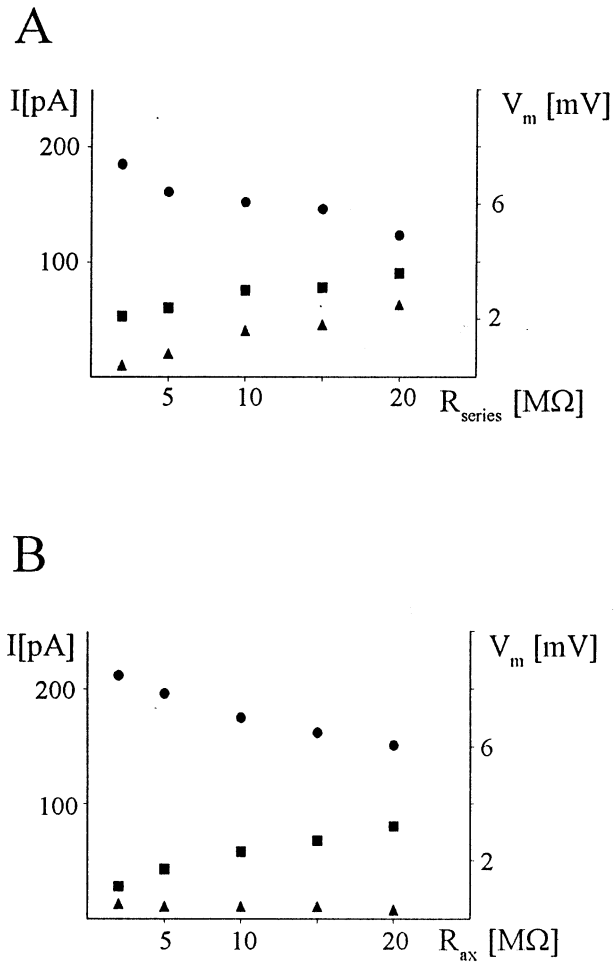

Fig. 7. Dependence of synaptic current amplitude (●), somatic (▲) and dendritic (■) voltage escape on cellular architecture. (A) Increasing series resistance deteriorates both somatic and dendritic VC in recordings with a continuous feedback amplifier. (B) Increase in R_{ax} reveals decreasing current amplitude, increasing dendritic voltage escape but almost constantly good somatic voltage clamp (dSEVC recording).

Recordings with a dSEVC are nominally independent from R_{series}. Moreover, the amplifier's potential output provides information about the true intracellular potential given that the electrode capacitance has been optimally compensated (Polder et al., 1984). Even in such recordings, the pipette is usually located at the cell soma and the voltage in remote cellular compartments remains unknown. Our recordings with a two-compartment model allow for the direct observation of the 'dendritic' voltage and are, therefore, a hardware realization of the 'two patch model' computed by Armstrong and Gilly (1992). Again, the test cell could be used to demonstrate the effect of changes in R_m or in cell geometry, e.g. by changing the axial resistance, R_{ax}.

Lastly, we used the model for the demonstration of typical problems arising from VC recording of synaptic currents. Very fast or remotely located postsynaptic conductance changes can be considerably slowed down in VC recordings or—in the worst case—can appear unrealistically fast and large due to the activation of voltage-activated ion channels by the synaptic voltage escape. Several authors have addressed this problem using computer simulations of branched cells either in compartment models (Johnston and Brown, 1983; De Schutter and Bower, 1994; Henze et al., 1996) or in continuous models based on cable theory (Major, 1993; Spruston et al., 1993). The hardware model presented here is ideally suited to induce defined conductance changes in single compartments by adequate changes of $V(R)$. Following a triangular change in $V(R)$ we found an almost linear current response showing that within the range of conductance values tested here the simulated membrane conductance follows $U(R)$ largely linearly (conductance g proportional to I at constant potential, Ohm's law). Again, the voltage escape in each compartment can be immediately controlled. We used the model to demonstrate the effect of series resistance changes in recordings with a cPCA and of varying electrotonic distance between soma and dendrite with a dSEVC. We also used the test cell for direct comparison of VC vs. CC recordings demonstrating the unsatisfying potential control of remote synaptic inputs.

In summary, the model cell presented here is a useful tool to demonstrate basic biophysical properties of simple and complex cells and to assess the quality of VC recordings with different amplifiers or different cell geometries. It can, therefore, be used to decide for the optimal amplifier design for a planned experiment (for theoretical comparison of cPCA and dSEVC see Sala and Sala, 1994) or to optimize the amplifier tuning in certain recording situations. Our hardware model can even be used in conjunction with real microelectrodes to analyse individual recording situations. The electrode is then immersed in the bath as deep as during the experiment and the cell model is connected between the bath and ground. With this approach the specific restrictions arising from certain recording situations can be directly observed. Indeed, a similar model has already been used by Richter et al. (1996) to validate the performance of a dSEVC with extremely deep immersed intracellular electrodes in vivo. Future applications of the test cell might also simulate more complex and realistic models of neurons. It has recently been shown that many active and passive properties of neurons can be simulated by highly reduced models involving nine or less compartments (Bush and Sejnowski, 1993; Mainen and Sejnowski, 1996). The present cell model can easily be extended to this size by connecting various elements and therefore might bridge the gap between real recording situations and computer models.

Acknowledgements

The authors gratefully acknowledge the assistance of M. Friedrich in construction and tuning of the cell model. We thank Dr H.-J. Gabriel for expert advice and helpful discussions.

References

Armstrong, CM and Gilly, WF. Access resistance and space clamp problems associated with whole-cell patch clamping. In: Methods in Emzymology, Vol. 207, Academic Press, San Diego, CA, USA, 1992.

Bekkers JM, Stevens CF. Cable properties of cultured hippocampal neurons determined from sucrose-evoked miniature EPSCs. J Neurophysiol 1996;75:1250–5.

Brennecke R, Lindemann B. Theory of a membrane-voltage-clamp with discontinuous feedback through a pulsed current-clamp. Rev Sci Instrum 1974;45:184–8.

Bush PC, Sejnowski TJ. Reduced compartmental models of neocortical pyramidal cells. J Neurosci Methods 1993;46:159–66.

De Schutter E, Bower JM. An active membrane model of the cerebellar purkinje cell. II. Simulation of synaptic responses. J Neurophysiol 1994;71:401–19.

Hamill OP, Marty A, Neher E, Sakmann B, Sigworth FJ. Improved patch-clamp techniques for high-resolution current recording from cells and cell-free membrane patches. Pflügers Arch 1981;391:85–100.

Henze DA, Cameron WE, Barrionuevo GN. Dendritic morphology and its effects on the amplitude and rise-time of synaptic signals in hippocampal CA3 pyramidal cells. J Comp Neurol 1996;369:331–44.

Johnston D, Brown TH. Interpretation of voltage-clamp measurements in hippocampal neurons. J Neurophysiol 1983;50:464–86.

Mainen ZF, Sejnowski TJ. Influence of dendritic structure on firing pattern in model neocortical neurons. Nature 1996;382:363–6.

Major G. Solutions for transients in arbitrarily branching cables: III. Voltage clamp problems. Biophys J 1993;65:469–91.

Marty, A and Neher, E. Tight-seal whole-cell recording. In: Sakmann B and Neher E, editors. Single Channel Recording, 2nd edition, Plenum Press, New York, 1995.

Müller W, Lux HD. Analysis of voltage-dependent membrane currents in spatially extended neurons from point-clamp data. J Neurophysiol 1993;69:241–7.

Ogden, D and Stanfield, P. Patch clamp techniques for single channel and whole-cell recording. In: Ogden D, editor. Microelectrode Techniques, 2nd edition, The Company of Biologists Ltd., Cambridge, 1994.

Polder HR, Swandulla D, Konnerth A, Lux HD. An improved high current single electrode current/voltage clamp system. Pflügers Arch. 1984;406:R43.

Richter DW, Pierrefiche O, Lalley PM, Polder HR. Voltage-clamp analysis of neurons within deep layers of the brain. J Neurosci Methods 1996;67:121–31.

Sahm III, WH and Smith, MW, editors. Optoelectronics Manual. 3rd edition, General Electric Company, Auburn, Auburn, NY, USA, 1984.

Sala F, Sala S. Sources of error in single-electrode voltage-clamp techniques: a computer simulation study. J Neurosci Methods 1994;53:189–97.

Sigworth, FJ. Electronic design of the patch-clamp. In: Sakmann B and Neher E, editors. Single Channel Recording, 2nd edition, Plenum Press, New York, 1995.

Spruston N, Jaffe DB, Williams SH, Johnston D. Voltage- and space-clamp errors assocoated with the measurement of electrotonically remote synaptic events. J Neurophysiol 1993;70:781–802.

Staley KJ, Otis TS, Mody I. Membrane properties of dentate gyrus granule cells: comparison of sharp microelectrode and whole-cell recordings. J Neurophysiol 1992;67:1346–58.

Silver RA, Traynella SF, Cull-Candy SG. Rapid time-course miniature and evoked excitatory currents at cerebellar synapses in situ. Nature 1992;355:163–6.

Williams SH, Johnston D. Kinetic properties of two anatomically distinct excitatory synapses in hippocampal CA3 pyramidal neurons. J Neurophysiol 1991;66:1010–20.

Wilson WA, Goldner MM. Voltage clamping with a single microelectrode. J Neurobiol 1975;6:411–22.